Electronic Supplementary Information

Manipulating selective amines transformation pathway via cocatalyst-modified monolayer $ZnIn_2S_4$ photocatalyst

Jian-Hui Zheng[a], Ming-Yu Qi[a], Zi-Rong Tang*[a], Yi-Jun Xu*[a]

[a]*College of Chemistry, State Key Laboratory of Photocatalysis on Energy and Environment,*
Fuzhou University, Fuzhou 350116, P.R. China

**To whom correspondence should be addressed. Tel. /Fax: +86 591 22865836;*
E-mail: zrtang@fzu.edu.cn; yjxu@fzu.edu.cn

Contents list

Fig. S19. Mott Schottky plots for (a) Cu_2S, (b) ZIS and Cu_2S/ZIS.

Table S1. Controlled experiment results for photocatalyzed-redox reaction of benzylamine on RuS_2/ZIS.

Table S2. Controlled experiment results for photocatalyzed-redox reaction of benzylamine on Cu_2S/ZIS.

Experimental procedures

Characterization methods. The X-ray diffraction (XRD) patterns of the samples were measured on a Rigaku Miniflex diffractometer with Cu Kα radiation. X-ray photoelectron spectroscopy (XPS) measurements were performed using a Thermo Scientific ESCA Lab250 spectrometer, and all of the binding energies were calibrated by the C 1s peak at 284.8 eV. UV-vis diffuse reflectance spectroscopy (DRS) on UV-vis Spectrophotometers (Thermo Scientific Evolution 200 Series) was used to measure the optical properties of the samples with $BaSO_4$ as the internal reflectance standard. The morphology of the samples was analyzed by scanning electron microscopy (SEM) on a FEI Nova NANO-SEM 230 spectrophotometer. The morphology and elemental distribution of the samples were analyzed by transmission electron microscopy (TEM), high-resolution TEM (HR-TEM), and elements mapping analysis using a JEOL model JEM 2010 EX instrument at an accelerating voltage of 200 kV. The Atomic force microscopy (AFM) patterns of the samples were measured on a Bruker Dimension ICON electron microscope. The Fourier transformed infrared spectroscopy (FTIR) was performed on a Thermo Scientific Nicolet iS 50 FT-IR spectrophotometer. Electron paramagnetic resonance (EPR) spectroscopic measurements were performed at room temperature using a Bruker A300 EPR spectrometer. For in situ EPR measurements, 5 mg sample powders were dispersed in a mixed solution of 10 mL CH_3CN containing 0.2 mmol BA and DMPO (0. 5 mmol), which was used as a spin-trapping agent, by ultrasonic treatment. Then, the suspension was injected into a glass capillary and the glass capillary was placed in a sealed glass tube under the argon (Ar) atmosphere. The sealed glass tube was placed in the microwave cavity of the EPR spectrometer and was irradiated with a 300 W Xe lamp (> 420nm) during EPR measurements at room temperature. The photoelectrochemical analysis was carried out on Autolab M204 workstation in a conventional three-electrode cell using a Pt plate and an Ag/AgCl electrode as the counter electrode and reference electrode, respectively. FTO glass was used as support to prepare working electrode. Specifically, the slurry prepared by dispersing 5 mg sample in 0.5 mL of DMF and 50 μL of Nafion solution was spread onto FTO glass with an exposed area of 0.25 cm^2. After air drying, the working electrodes were dried at 60°C for 2 h to enhance adhesion. The photoluminescence (PL) spectra for samples were analyzed on an Edinburgh Analytical Instrument F900 spectrophotometer with an excitation wavelength of 360 nm. To ensure the comparability of the PL spectra, the experimental parameters, including the excitation wavelength, slit width, and the amount of the samples, were identical.

Determination of apparent quantum yield (AQY). The AQY of H_2 for the RuS_2/ZIS composites was measured under the same reaction conditions with irradiation light through different wavelength band-pass filter (430, 450, 500, 600 nm). The photon flux of incident light was measured by a PL-MW2000 photoradiometer (Perfectlight, Beijing, China). The AQY was calculated according to the following equation:[1]

$$\mathrm{AQY} = \frac{N_e}{N_p} \times 100\% = \frac{2 \times M \times N_A \times h \times c}{S \times P \times t \times \lambda} \times 100\%$$

where N_h is the number of reaction holes, N_p is the number of incident photons, M is the molar amount of HB, N_A is Avogadro constant, h is the Planck constant, c is the speed of light, S is the irradiation area, P is the light powerdensity, t is the reaction time and λ is the incident light wavelength.

Photocatalytic recycling tests. To evaluate the photocatalytic stability of the catalyst, four recycling tests were carried out and detailed experimental procedures were shown as follows. After the photocatalytic reaction of the first run, the catalysts were separated and rinsed by DI water three times. Afterward, the second cycle test is carried out by mixing fresh CH_3CN solution containing 0.2 mmol BA with the used catalyst. The subsequent recycling tests were executed in an analogous pattern.[2]

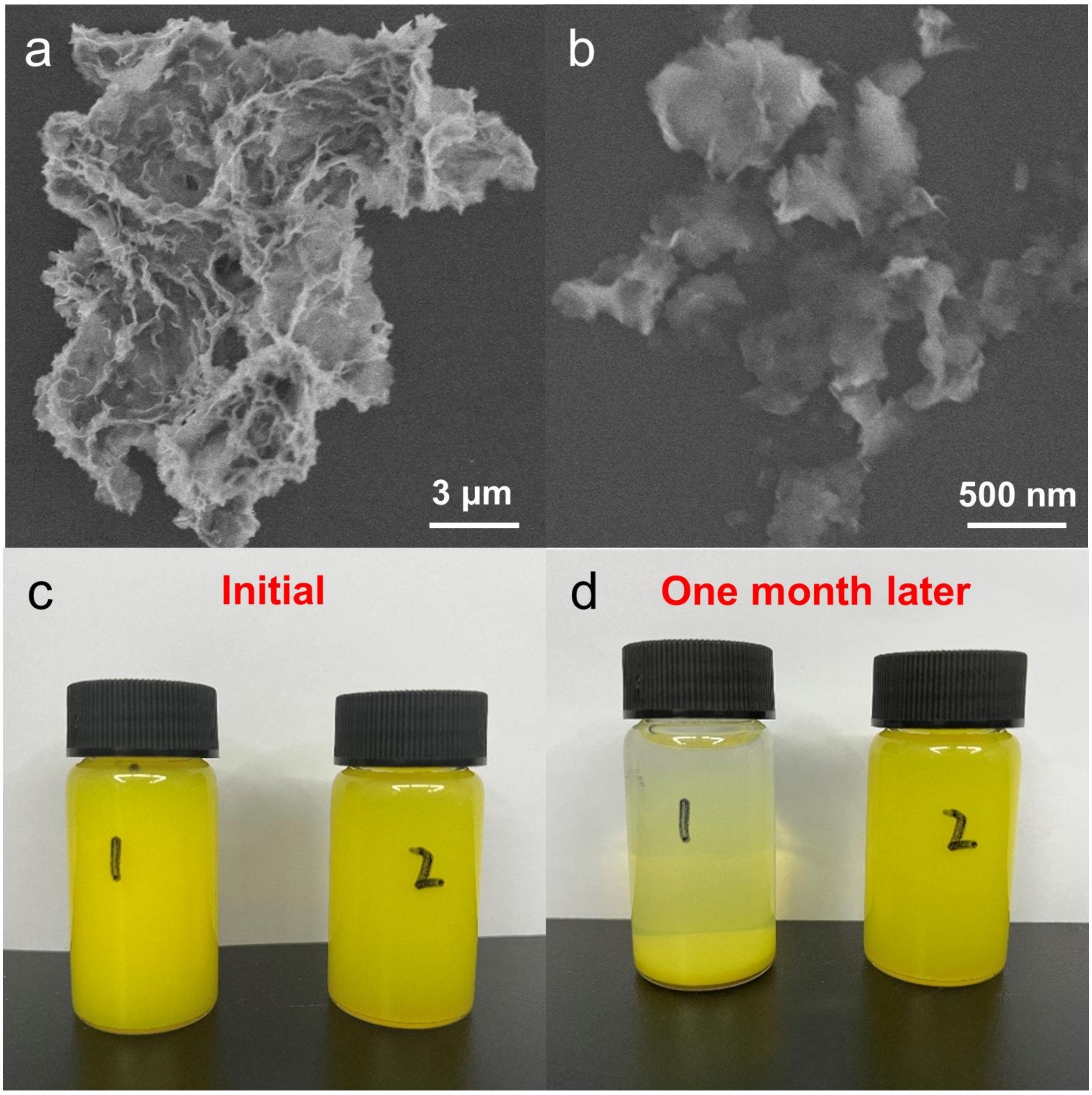

Fig. S1. (a) SEM image of bulk ZIS. (b) SEM image of single-unit-cell-layer ZIS. (c, d) Suspensions image of bulk ZIS (Bottle 1) and single-unit-cell-layer ZIS (Bottle 2).

Note: As shown in **Fig. S1a and b**, the bulk ZIS is exfoliated to present a smaller size thin sheet state. The exfoliated ZIS can be well dispersed in water for a long time, which compounds the properties of monolayer or few layer materials.[3]

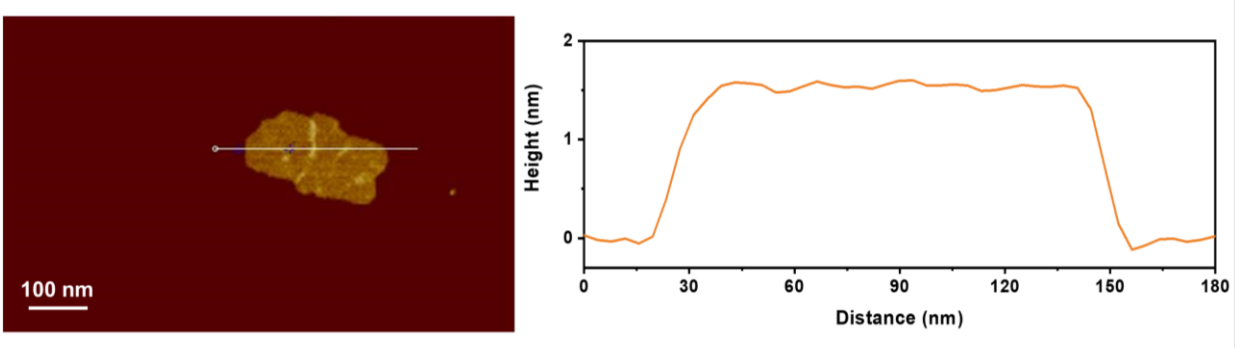

Fig. S2. AFM image and the corresponding height profile of ZIS.

Note: The test result of ZIS is close to the parameters of semicrystalline cells (single cell c parameter is about 2.5 nm),[4] indicating that the bulk ZIS is effectively stripped into a monolayer structure.

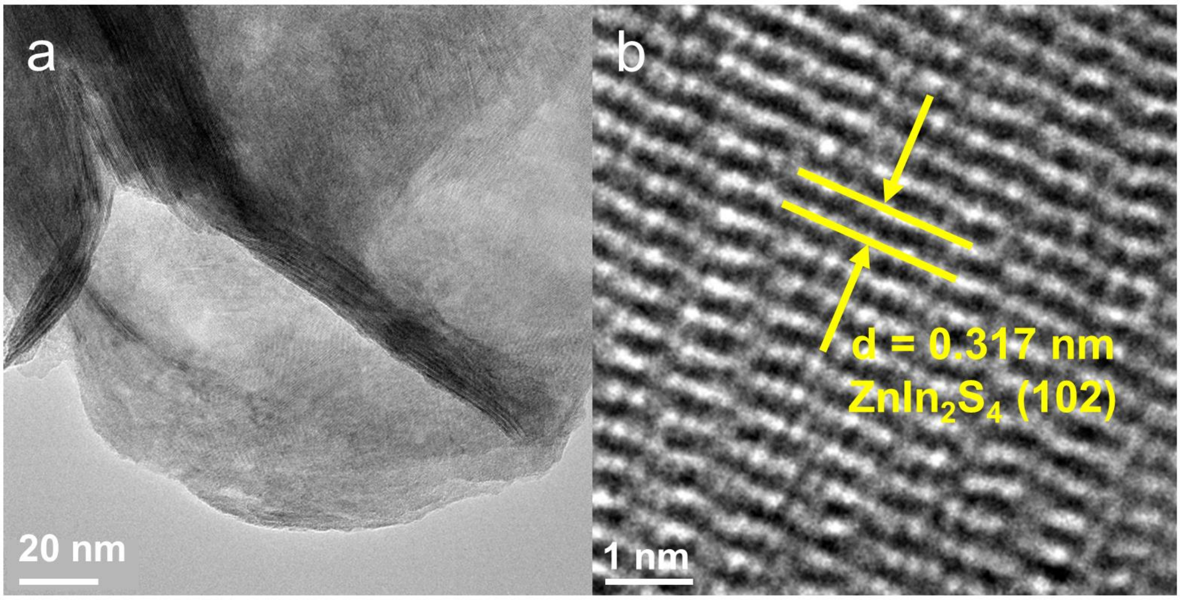

Fig. S3. (a) TEM image and (b) HRTEM image of ZIS.

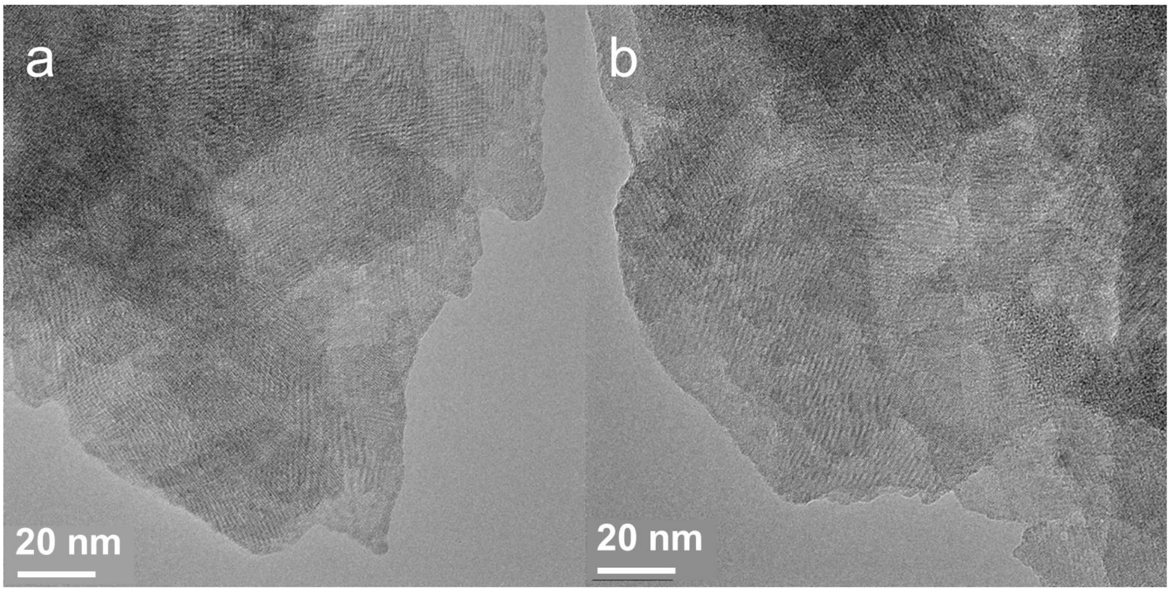

Fig. S4. (a) TEM image of Cu_2S/ZIS. (b) TEM image of RuS_2/ZIS.

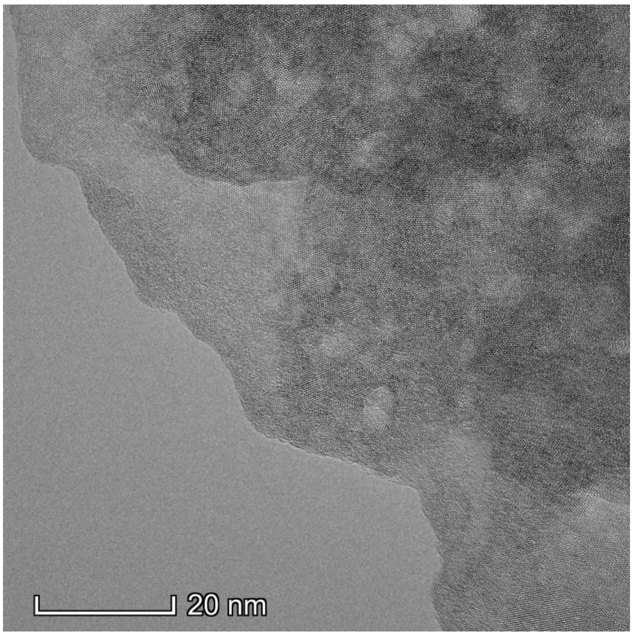

Fig. S5. HRTEM image of ZIS image of RuS_2/ZIS.

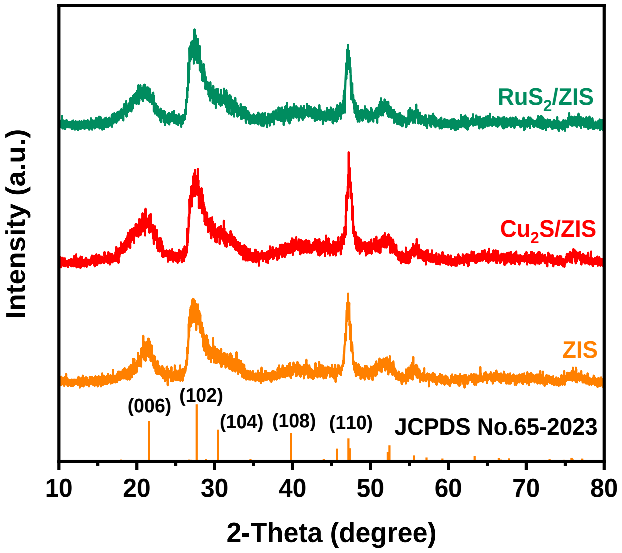

Fig. S6. XRD patterns of ZIS, Cu_2S/ZIS and RuS_2/ZIS.

Note: The XRD spectra of pure ZIS are consistent with hexagonal phase ZIS (JCPDS No. 65-2023).[5] There is no significant change in the characteristic peaks in the XRD spectra of the composites, which may be related to the low content, small nanometer size and uniform dispersion of the metal sulfides in the composites.

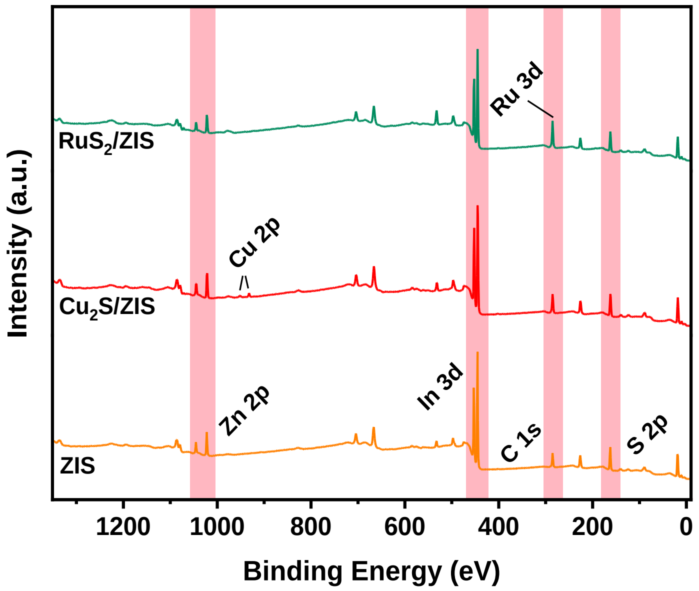

Fig. S7. XPS survey spectra of ZIS, Cu_2S/ZIS and RuS_2/ZIS.

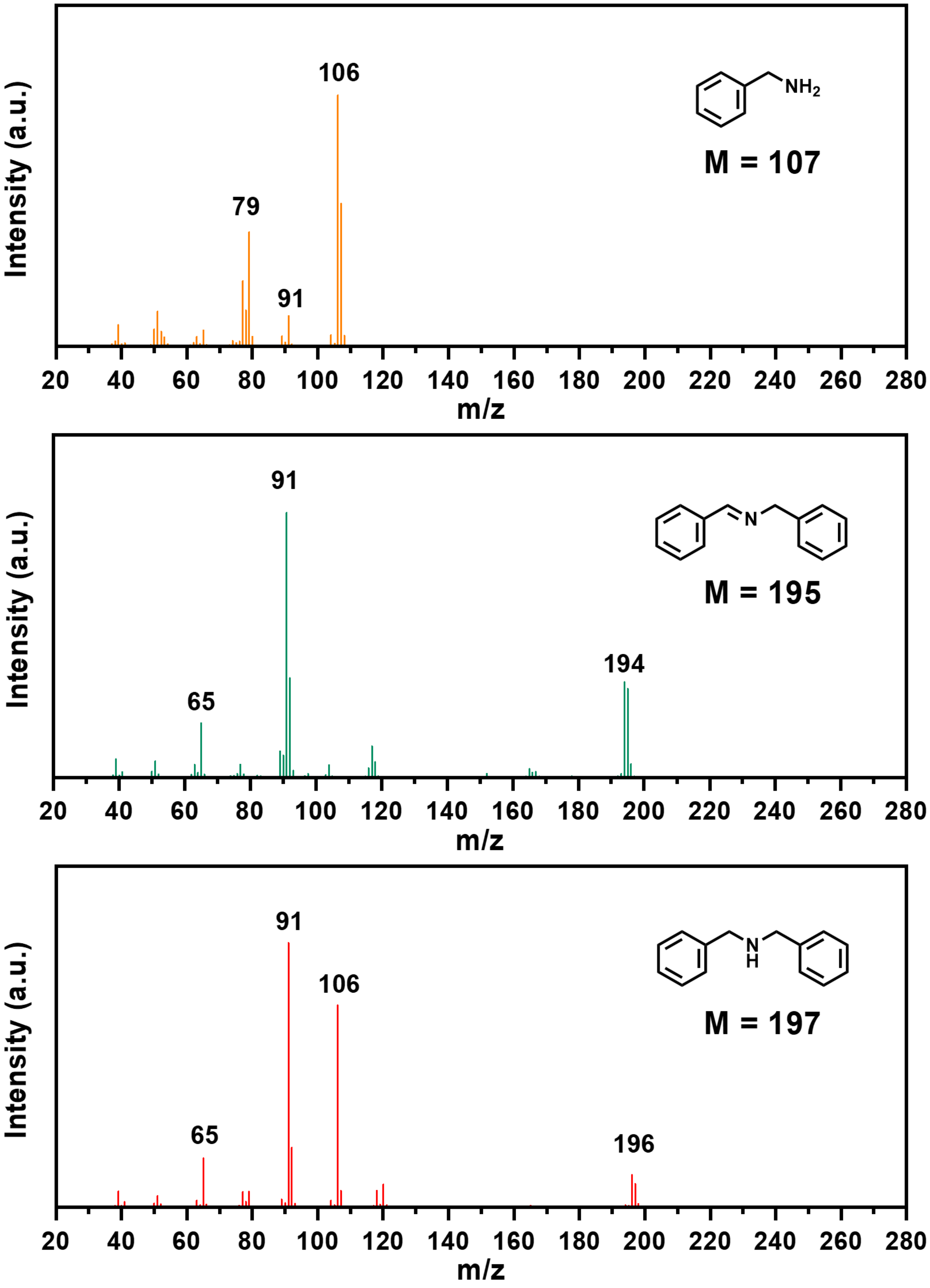

Fig. S8. Mass spectra of BA (feedstock) and the obtained liquid products NBBA and DBA catalyzed by RuS_2/ZIS and Cu_2S/ZIS, respectively.

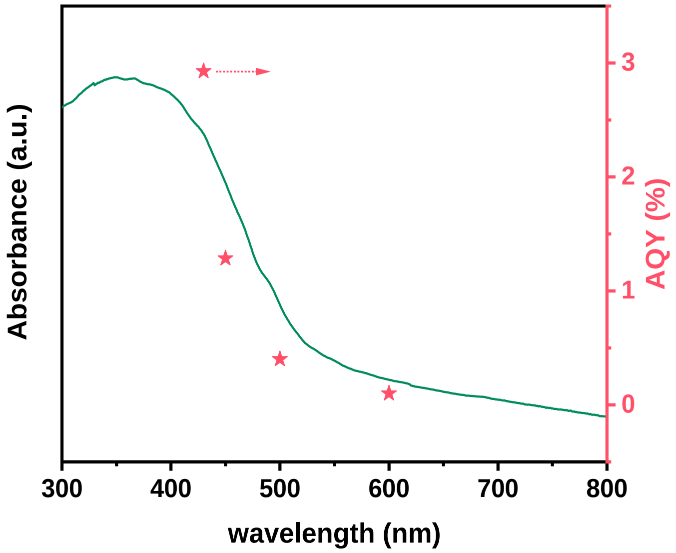

Fig. S9. DRS spectrum of RuS_2/ZIS and AQYs for H_2 production over RuS_2/ZIS under different monochromatic lights.

Note: The apparent quantum yields (AQYs) for the RuS_2/ZIS, calculated as the number of charge carriers (electrons) used for the H_2 production divided by the number of incident photons, depend strongly on the light wavelength and match well with the DRS spectrum for the RuS_2/ZIS, further suggesting that this dual-functional catalytic reaction is initiated by light excitation of ZIS.

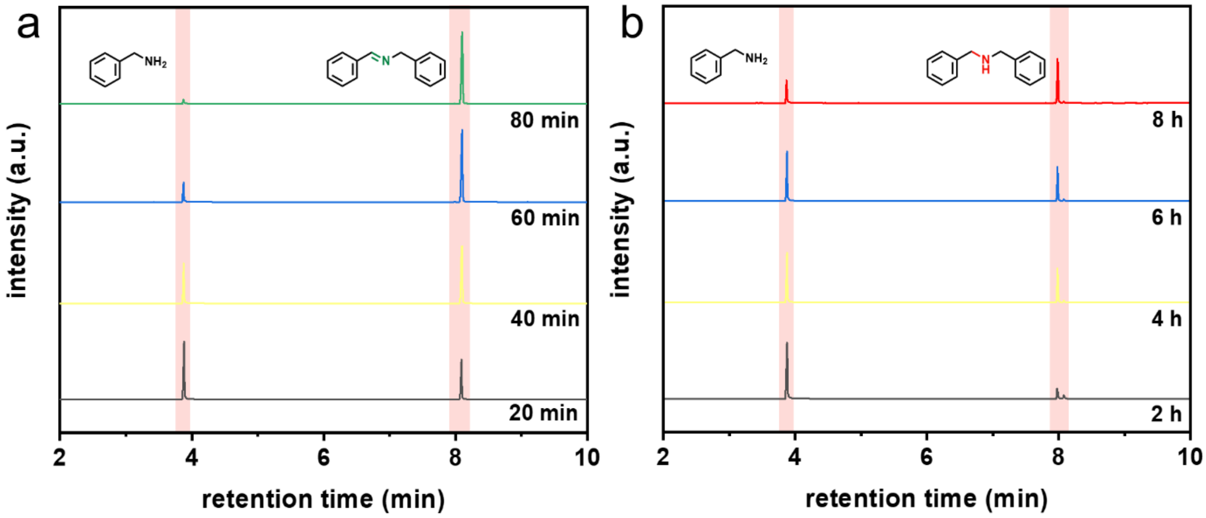

Fig. S10. GC chromatograms of liquid reaction mixtures collected at different reaction times in the presence of (a) RuS_2/ZIS and (b) Cu_2S/ZIS.

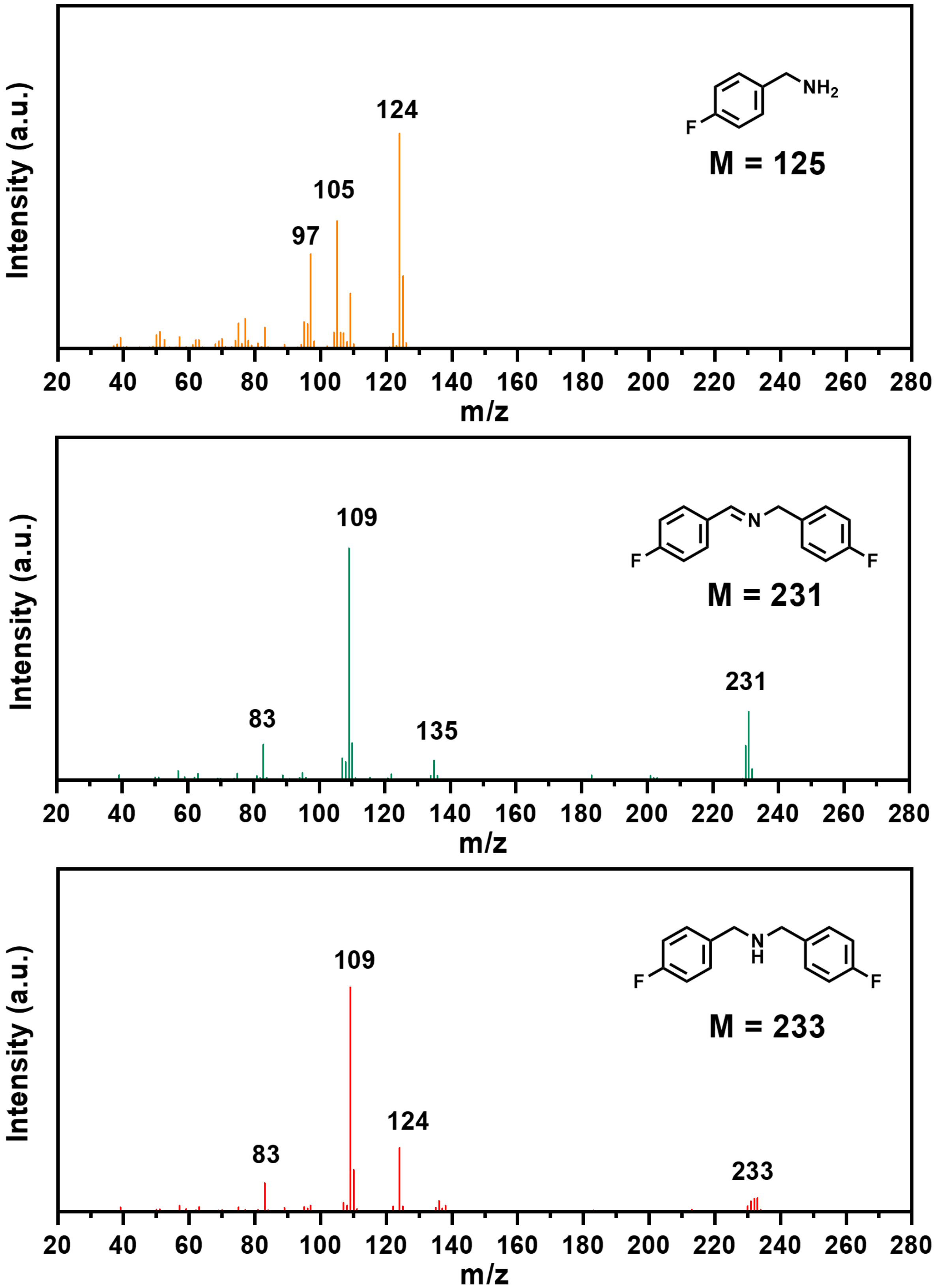

Fig. S11. Mass spectra of 4-Fluorobenzylamine and corresponding liquid products catalyzed by RuS_2/ZIS and Cu_2S/ZIS, respectively.

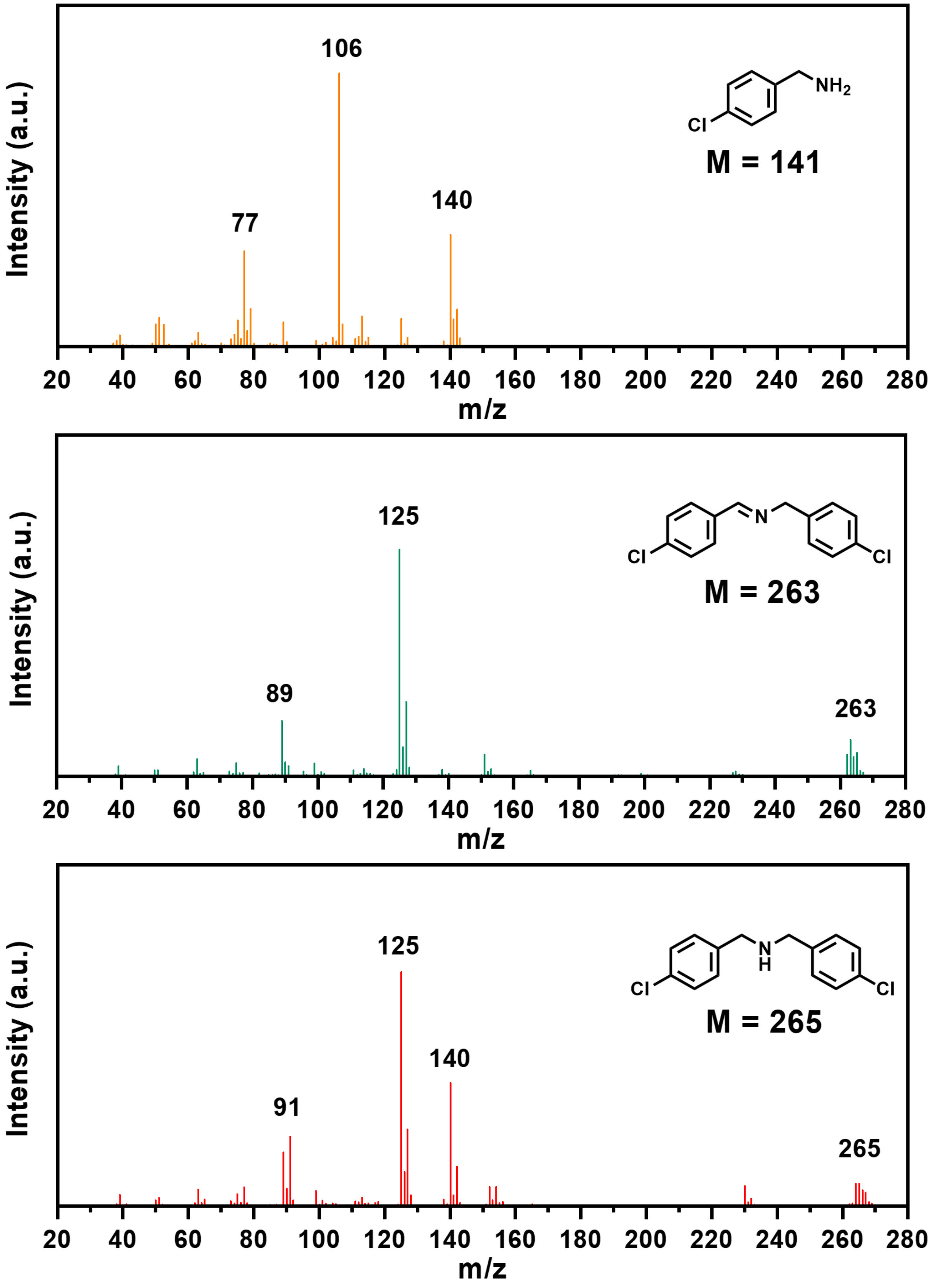

Fig. S12. Mass spectra of 4-Chlorobenzylamine and corresponding liquid products catalyzed by RuS_2/ZIS and Cu_2S/ZIS, respectively.

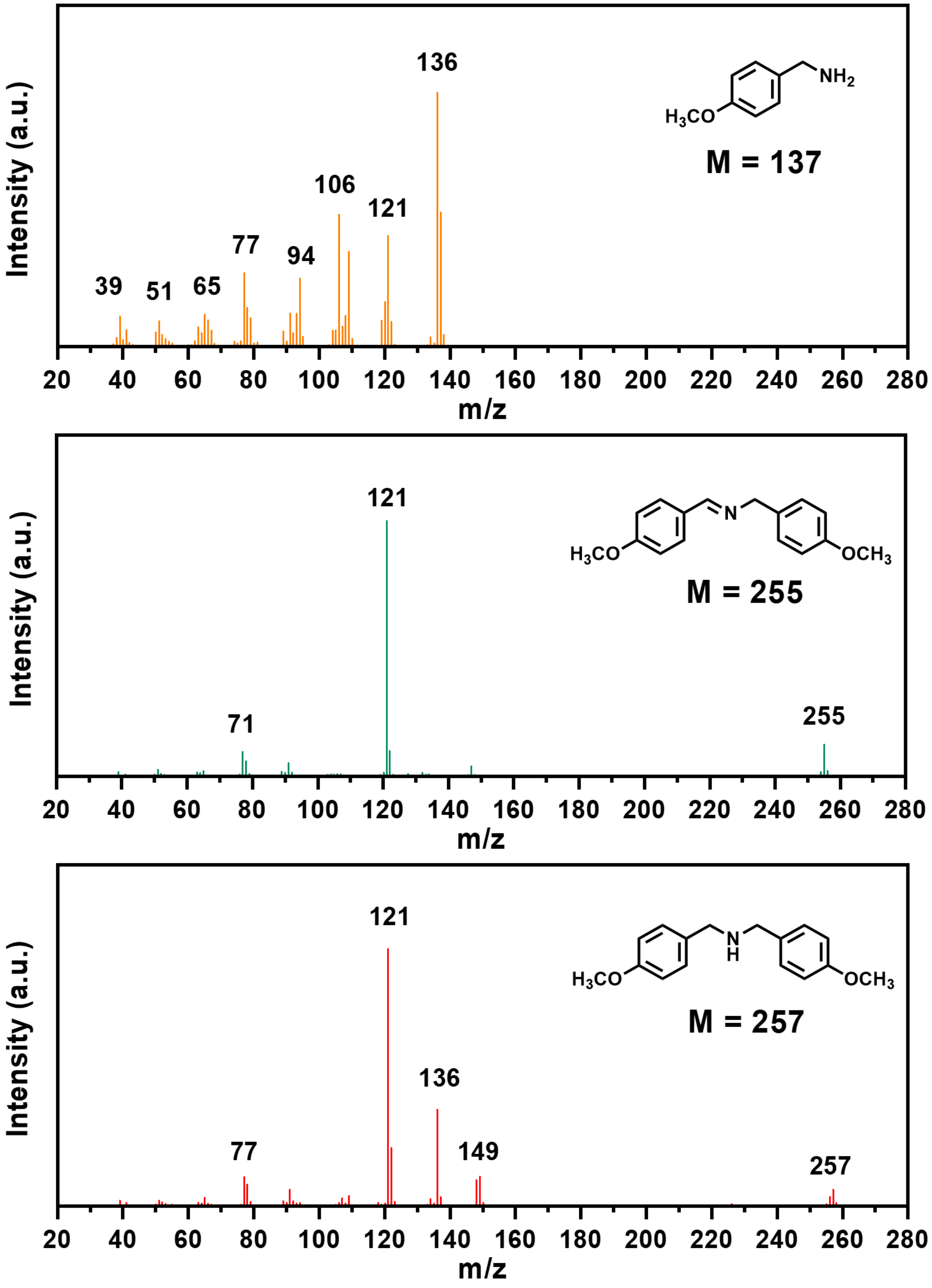

Fig. S13. Mass spectra of 4-Methoxybenzylamine and corresponding liquid products catalyzed by RuS_2/ZIS and Cu_2S/ZIS, respectively.

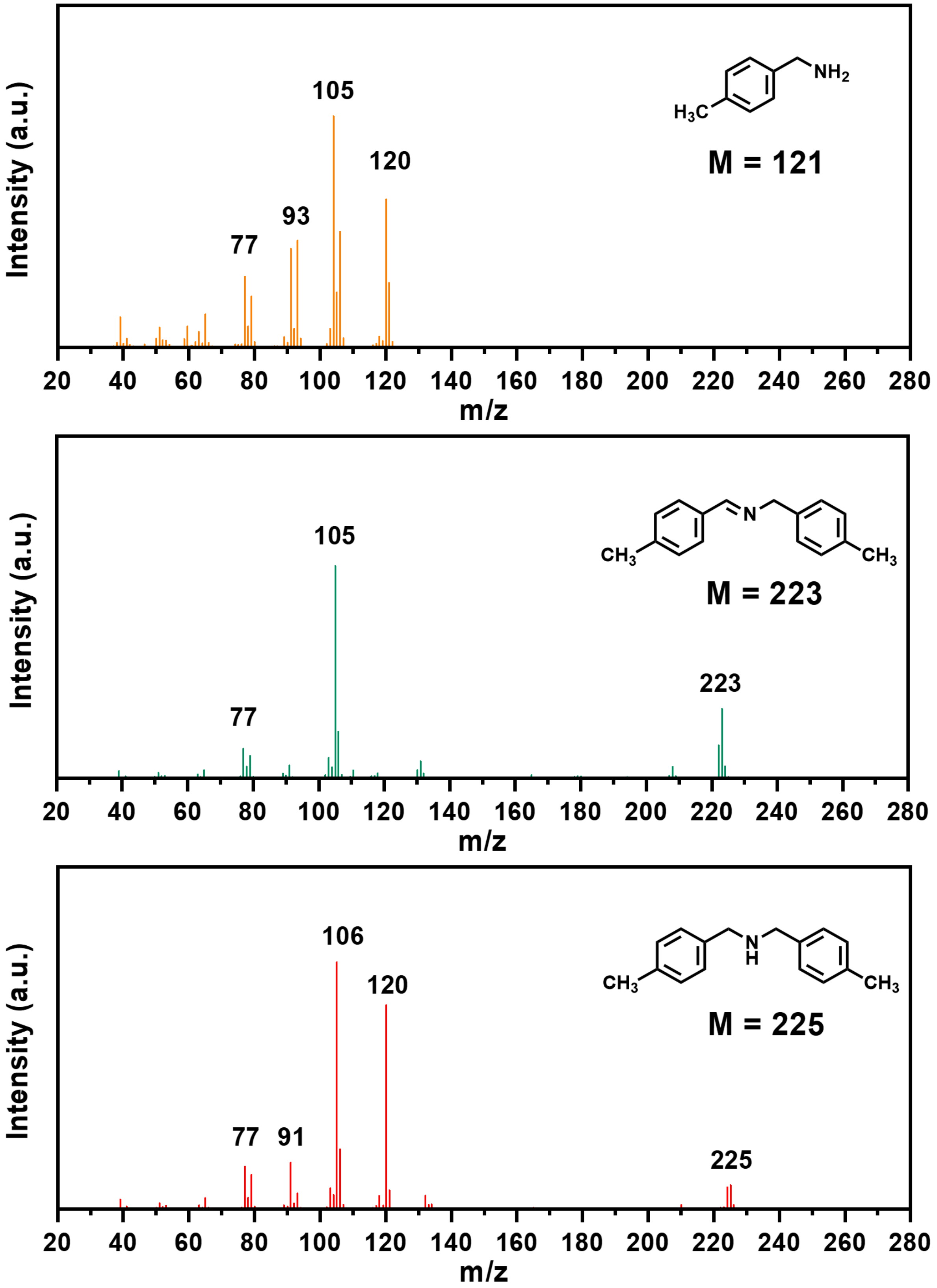

Fig. S14. Mass spectra of 4-Methylbenzylamine and corresponding liquid products catalyzed by RuS_2/ZIS and Cu_2S/ZIS, respectively.

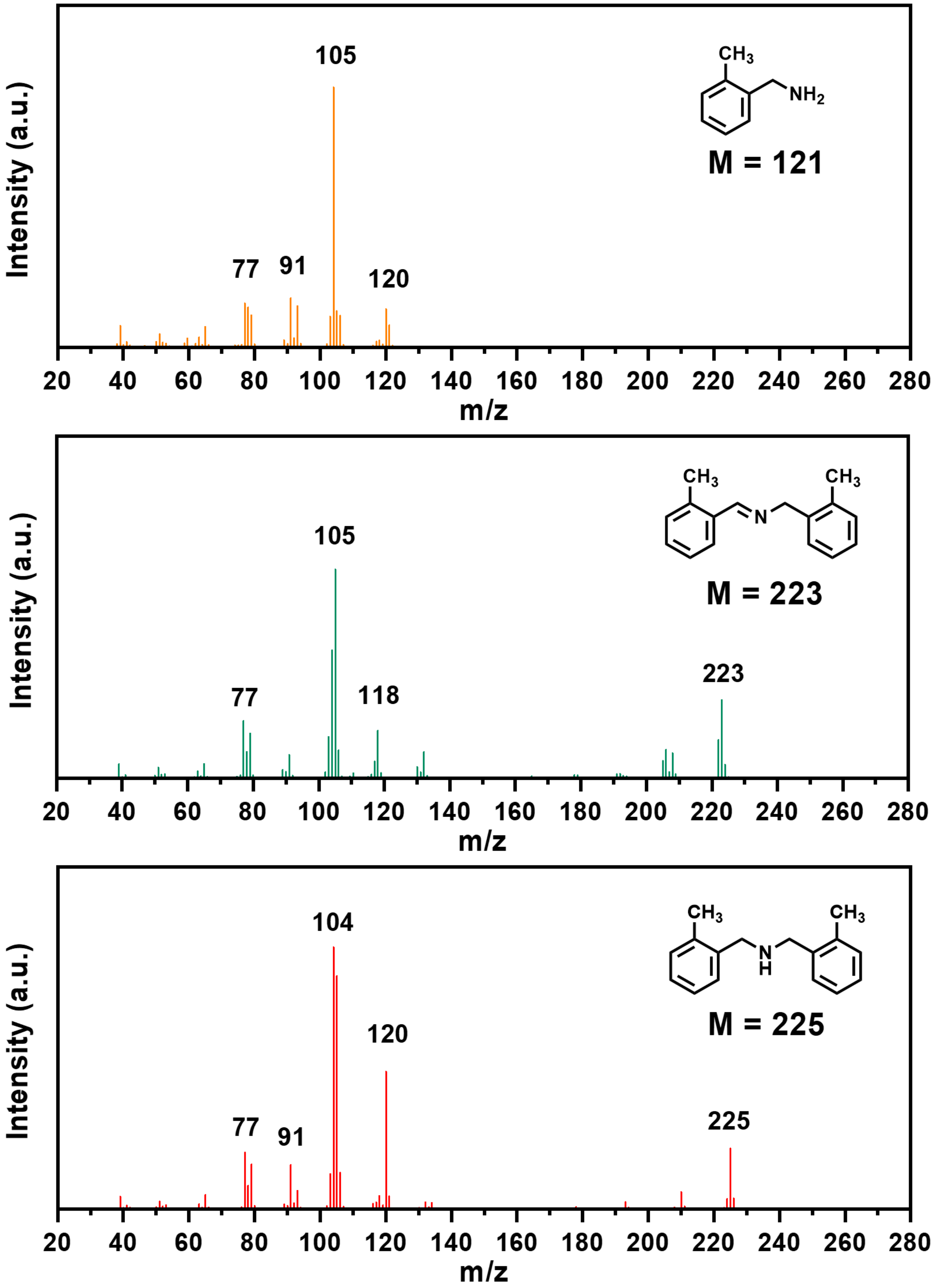

Fig. S15. Mass spectra of 2-Methylbenzylamine and corresponding liquid products catalyzed by RuS_2/ZIS and Cu_2S/ZIS, respectively.

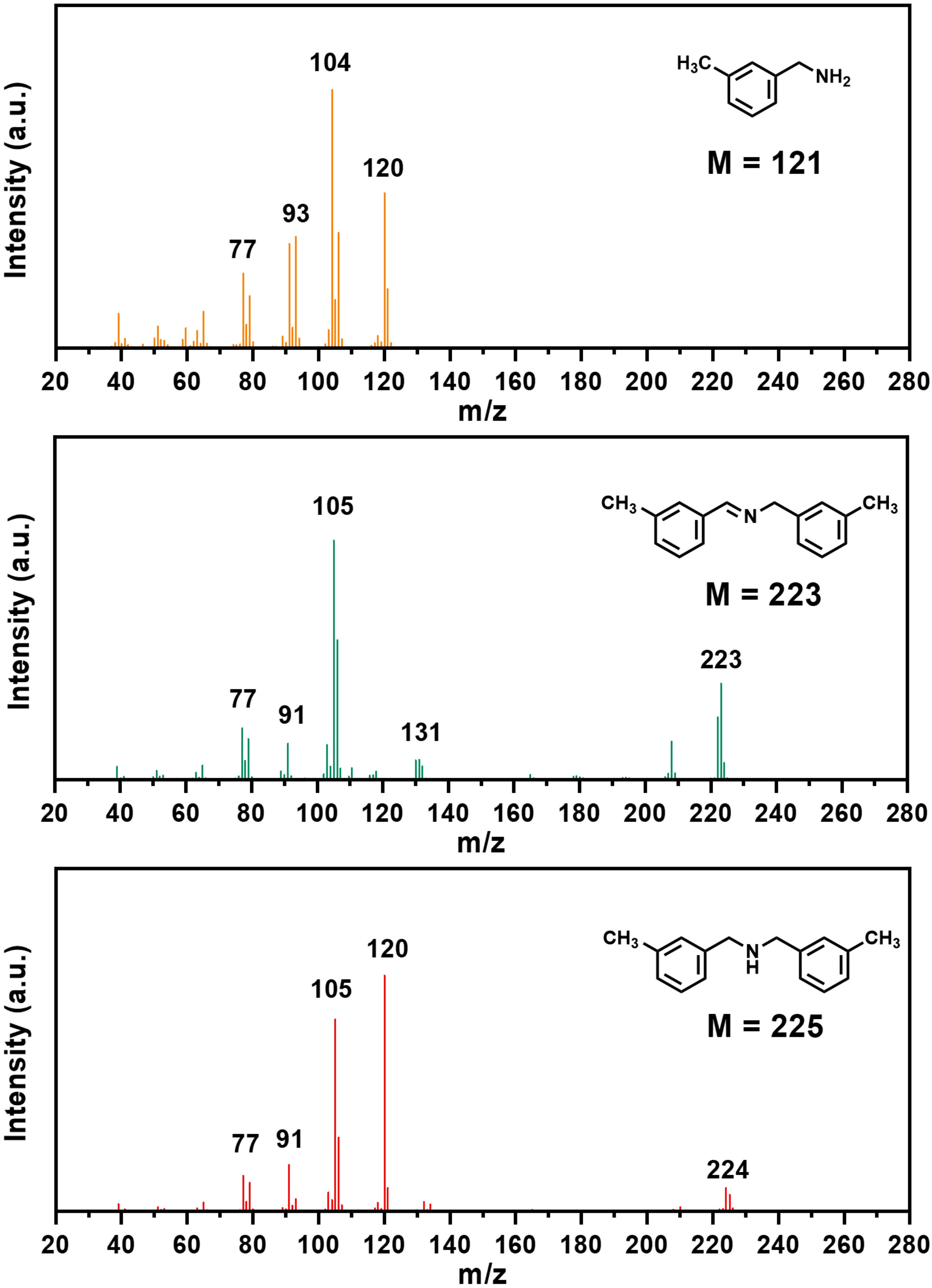

Fig. S16. Mass spectra of 3-Methylbenzylamine and corresponding liquid products catalyzed by RuS_2/ZIS and Cu_2S/ZIS, respectively.

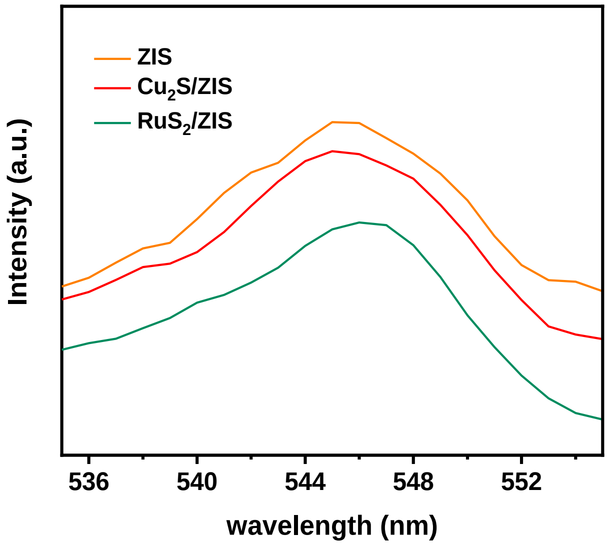

Fig. S17. The photoluminescence (PL) emission spectra (λ_{ex} = 360 nm) of ZIS, Cu_2S/ZIS and RuS_2/ZIS.

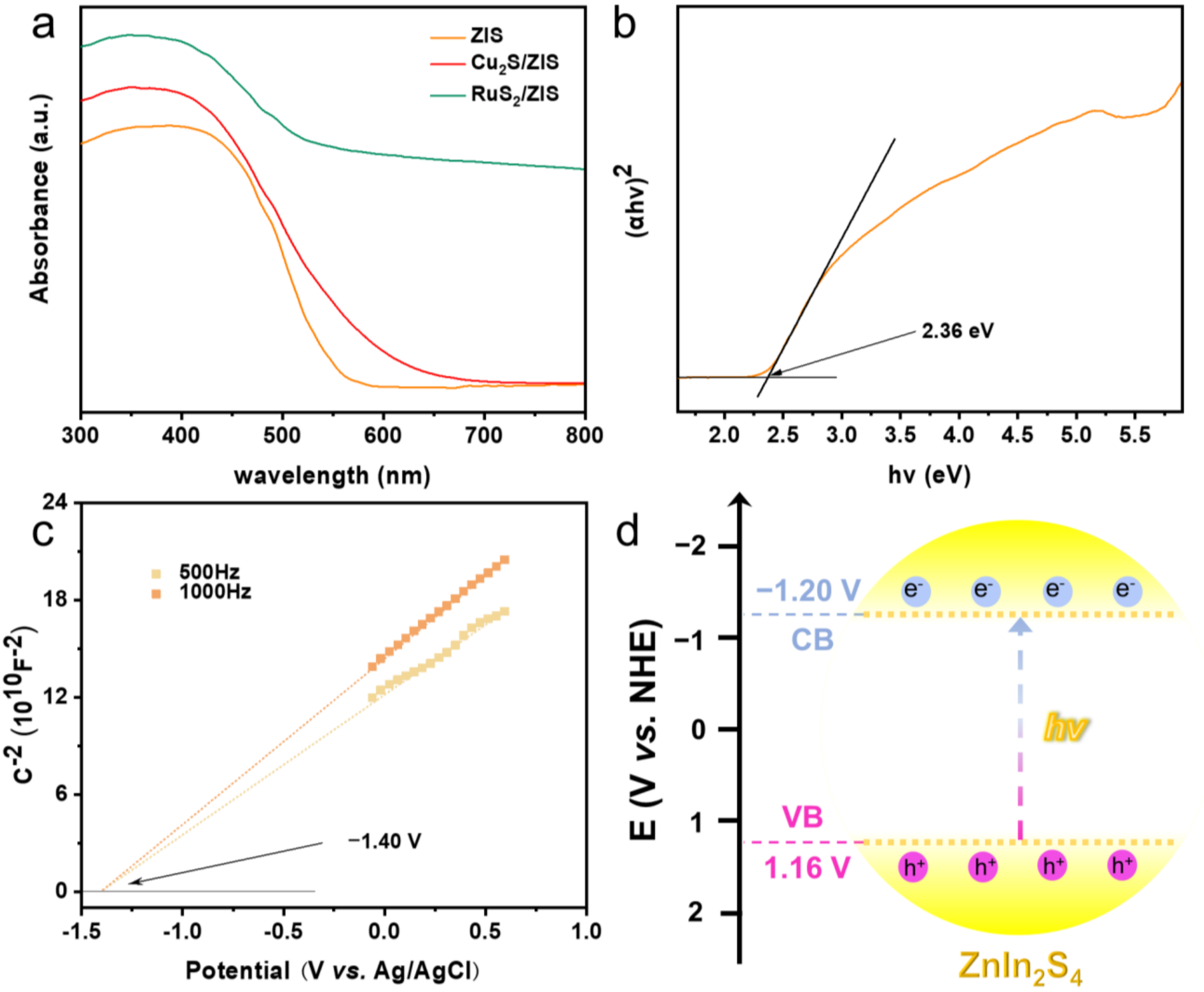

Fig. S18. (a) DRS spectra of ZIS, Cu_2S/ZIS and RuS_2/ZIS. (b) Tauc plots for the optical band gap of ZIS. (c) Mott-Schottky plots for ZIS. (d) Valence band (VB) and conduction band (CB) positions of ZIS.

Note: To calculate the band gap energy, the following formula is used:

$$(Ah\nu)^n = K \cdot (h\nu - E_g)$$ [6]

where A is the absorption coefficient, hν is the photon energy, K is a constant, E_g is the band gap energy and n = 2 which corresponds to direct semiconductors ZIS. As shown in **Fig. S18**b, the band gap of ZIS is evaluated to be 2.36 eV. In addition, the flat band potential which refers to the conduction band (CB) of ZIS is calculated to be −1.40 V (vs. Ag/AgCl). On the equation between the Ag/AgCl and normal hydrogen electrode (NHE), $E_{NHE} = E_{Ag/AgCl} + 0.197$ V, the CB values of ZIS is estimated to be −1.20 V *vs.* NHE. With the band gap of 2.36 eV determined from the above result, the valence band (VB) of ZIS is then calculated with the value of 1.16 V *vs.* NHE.

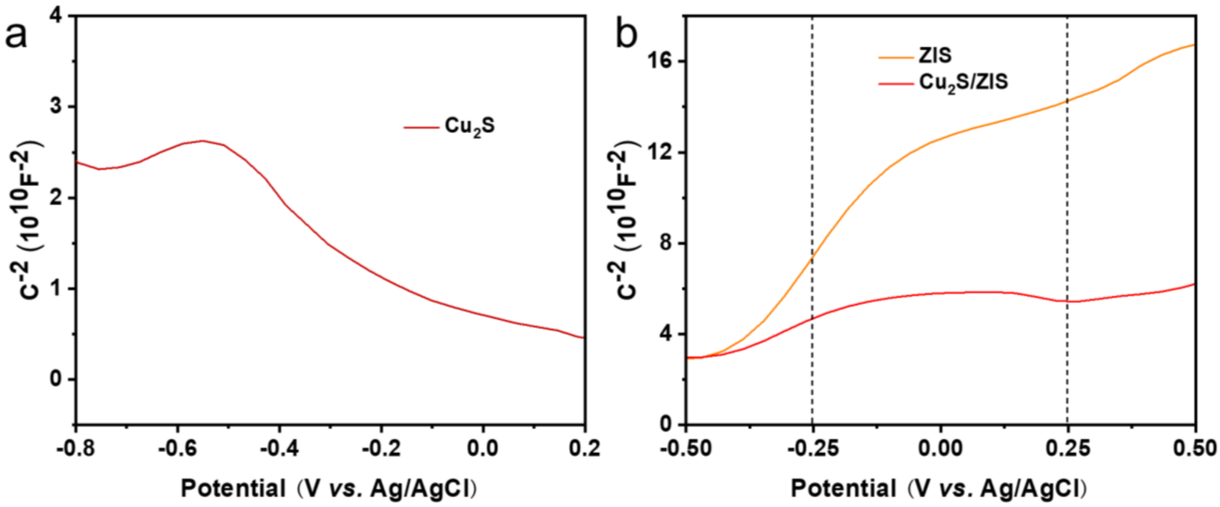

Fig. S19. Mott Schottky plots for (a) Cu_2S, (b) ZIS and Cu_2S/ZIS.

Note: The Mott–Schottky plots of Cu_2S and ZIS exhibit the negative and positive slopes, respectively, suggesting that the Cu_2S is a p-type semiconductor and the ZIS is an n-type semiconductor. For the Cu_2S/ZIS composite, it should be particularly noted in **Fig. S19b** that the Mott-Schottky plot is bent, forming an inverted "V-shape", thus indicating the formation of a p-n junction at the interface between Cu_2S and ZIS.[7, 8]

Table S1. Controlled experiment results for photocatalyzed-redox reaction of benzylamine on RuS$_2$/ZIS[a].

Entry	Catalyst	Light source	Quenchers	H_2 (μmol)	Liquid products (μmol)		Conversion (%)
					DBA	NBBA	
1	RuS$_2$/ZIS	+	–	83.45	0.25	85.88	82.16
2	RuS$_2$/ZIS	–	–	–	–	–	–
3	–	+	–	–	–	–	–
4[b]	RuS$_2$/ZIS	+	CCl_4	20.94	0	61.54	50.08
5[c]	RuS$_2$/ZIS	+	TEOA	32.14	0	21.74	10.52
6[d]	RuS$_2$/ZIS	+	DMPO	8.22	0	12.08	31.21

[a] Reaction conditions: 5 mg photocatalyst, 0.2 mmol benzylamine, 10 mL CH_3CN, quenchers (0.1 mmol), Ar atmosphere, 1 h. [b] CCl_4 as electron sacrificial agent for capturing photogenerated electrons, [c] TEOA as hole sacrificial agent for trapping photogenerated holes, [d] DMPO as radical scavenger. + means with light irradiation, – means without corresponding conditions or products.

Table S2. Controlled experiment results for photocatalyzed-redox reaction of benzylamine on Cu$_2$S/ZIS[a].

Entry	Catalyst	Light source	Quenchers	H_2 (μmol)	Liquid products (μmol)		Conversion (%)
					DBA	NBBA	
1	Cu$_2$S/ZIS	+	–	6.51	29.51	3.95	87.17
2	Cu$_2$S/ZIS	–	–	–	–	–	–
3	–	+	–	–	–	–	–
4[b]	Cu$_2$S/ZIS	+	CCl_4	0	0	24.64	88.32
5[c]	Cu$_2$S/ZIS	+	TEOA	16.50	2.42	31.89	39.93
6[d]	Cu$_2$S/ZIS	+	DMPO	0.50	0.76	43.00	67.70

[a] Reaction conditions: 5 mg photocatalyst, 0.2 mmol benzylamine, 10 mL CH_3CN, quenchers (0.1 mmol), Ar atmosphere, 6 h. [b] CCl_4 as electron sacrificial agent for capturing photogenerated electrons, [c] TEOA as hole sacrificial agent for trapping photogenerated holes, [d] DMPO as radical scavenger. + means with light irradiation, – means without corresponding conditions or product.

References

1 M.-Y. Qi, M. Conte, Z.-R. Tang and Y.-J. Xu, *ACS Nano*, 2022, **16**, 17444-17453.
2 F.-K. Shang, M.-Y. Qi, C.-L. Tan, Z.-R. Tang and Y.-J. Xu, *ACS Phys. Chem. Au*, 2022, **2**, 216-224.
3 M.-Q. Yang, Y.-J. Xu, W. Lu, K. Zeng, H. Zhu, Q.-H. Xu and G. W. Ho, *Nat. Commun.*, 2017, **8**, 14224.
4 C. Du, Q. Zhang, Z. Lin, B. Yan, C. Xia and G. Yang, *Appl. Catal., B*, 2019, **248**, 193-201.
5 C.-L. Tan, M.-Y. Qi, Z.-R. Tang and Y.-J. Xu, *Appl. Catal., B*, 2021, **298**, 120541.
6 Y.-H. Li, M.-Y. Qi, Z.-R. Tang and Y.-J. Xu, *J. Phys. Chem. C*, 2022, **126**, 1872-1880.
7 X. Lin, S.-H. Li, K.-Q. Lu, Z.-R. Tang and Y.-J. Xu, *New J. Chem.*, 2018, **42**, 14096-14103.
8 L. Li, X. Dai, D.-L. Chen, Y. Zeng, Y. Hu and X. W. Lou, *Angew. Chem., Int. Ed.*, 2022, **61**, e202205839.